Room-Temperature Electrodeposition of Mg Metal from Amide Salts Dissolved in Glyme-Ionic Liquid Mixture

Atsushi Kitada,[a,b] Yuu Kang,[a] Yoshiharu Uchimoto,[b,c,*] and Kuniaki Murase[a,b,*,z]

[a]*Department of Materials Science and Engineering, Kyoto University, Kyoto 606-8501, Japan*
[b]*JST-CREST, Kawaguchi, Saitama 332-0012, Japan*
[c]*Graduate School of Human and Environmental Studies, Kyoto University, Kyoto 606-8501, Japan*

The electrodeposition of Mg metal from an ionic liquid–glyme mixture was investigated at room temperature. The mixture contains a glyme, a simple amide salt $Mg(Tf_2N)_2$ (Tf = SO_2CF_3), and a quaternary-ammonium Tf_2N ionic liquid. Using the mixture bath, substantial cathodic electrodeposition of Mg at a large current density ($\sim$10 mA cm^{-2}) was observed, suggesting a change in coordination geometry around Mg^{2+} cation together with improved conductivity. By mixing diglyme, the conductivity increased by an order of magnitude (2.5 – 2.6 mS cm^{-1}) compared to the glyme-free ionic liquid (0.35 mS cm^{-1}) and the viscosity became as low as that of pure glyme. Additionally, potentiostatic electrolysis resulted in a non-dendritic thin film of elemental Mg with metallic luster.

Elemental magnesium (Mg) is anticipated as a negative electrode material for post lithium-ion secondary batteries because of its high-theoretical capacity (3839 mAh cm^{-3}), high negative electrode potential (–2.356 V vs. SHE) and natural abundance. Because aqueous electrolytes are not available for electrodeposition of Mg, as is also the case for Li, the electrochemistry of magnesium has been studied in aprotic organic solvents since the early 1900's.[1–6] As Mg ion batteries attract increasing interest, electrodeposition of Mg has been investigated over the last thirty years by several groups, using mainly electrolytes consisting of an ether solvent tetrahydrofuran (THF) and alkylmagnesium halides RMgX (R = alkyl, aryl groups; X = Cl, Br), and some reports indicate that addition of $AlCl_3$ to form an organo-halo-aluminate is effective in Mg deposition and/or dissolution.[7–16] However, THF is so volatile and alkylmagnesium halides react so vigorously with water that they cannot be used practically. Thus, both the solvents and solutes for Mg deposition baths should be altered in interests of safety.

Since ionic liquids (ILs) have attractive characteristics such as lower volatility, incombustibility, high ion conductivity, and electrochemical stability, several studies on the redox behaviors of metallic Mg using IL have been conducted. Some studies recommend decreasing the volatility and increasing conductivity by mixing ILs with THF solutions of RMgX, where reversible Mg deposition/dissolution at room temperature is reported.[17] Cheek et al. demonstrated the reversible process of Mg deposition/dissolution in THF-free IL solutions of RMgX at 150°C.[18] Alternative solvents include glymes because they have boiling points and flash points above 100°C and relatively low volatilities. Aurbach et al. showed the Mg deposition/dissolution cycle with high coulomb efficiency in the tetraglyme-Grignard mixture.[15] Nevertheless, these mixtures still remain dangerous for commercial use since they contain RMgX.

Deposition of elemental Mg without THF and/or RMgX has been reported.[18–24] Cheek et al. showed Mg deposition redox behavior at room temperature in an IL dissolving $Mg(ClO_4)_2$ or $MgCl_2$, although their reduction currents were significantly lower than that in RMgX-containing ILs.[18] Abe et al. demonstrated the reversible deposition/dissolution cycle of Mg with high coulombic efficiency in 2Me-THF where $MgBr_2$ dissolved.[19] In addition, they also showed that some kinds of glyme solution, where $MgCl_2$ and $AlCl_3$ were dissolved, gave reversible deposition/dissolution behavior at room temperature.[20] Nevertheless, the abovementioned Mg salts contain halide anions, which can form halogen gas through anodic oxidization.[18] Because halogen gases carry a high environmental burden, non-halide anion electrolytes such as $Mg(Tf_2N)_2$ are favorable. Although NuLi

et al. reported the reversible deposition/dissolution cycle of Mg in $Mg(Tf_2N)_2$-containing ILs,[21–24] subsequent studies by other groups have not reproduced their results,[14,18,25] indicating that their results of reversible deposition/dissolution are highly questionable.

In this paper, we studied the electrodeposition of Mg metal at room temperature from relatively safe electrolytes consisting of IL/diglyme mixture (1 : 4 by volume) dissolving a simple amide salt $Mg(Tf_2N)_2$. Addition of an ionic liquid as supporting electrolyte resulted in increased conductivity by an order of magnitude (2.5 – 2.6 mS cm^{-1}) compared to the IL-free diglyme solution (0.50 mS cm^{-1}). Although certain flammability and volatility still exist in the glyme solution with an IL additive, this plating bath enabled the deposition of a thin and adherent film of elemental Mg with a metallic luster on Cu substrate.

Experimental

Preparation of the baths.— Trimethyl-*n*-hexylammonium bis[(trifluoromethyl)sulfonyl]amide (TMHA-Tf_2N) was synthesized from TMHABr and LiTf$_2$N via metathesis as reported previously.[26] *N*-methyl-*N*-propylpiperidinium bis[(trifluoromethyl)sulfonyl]amide (PP13-Tf_2N) and battery-grade diethyleneglycol dimethylether i.e. diglyme (G2) were purchased from Kanto Chemical. Battery-grade $Mg(Tf_2N)_2$ was purchased from Kishida Kagaku. First, we made 0.5 mol dm^{-3} $Mg(Tf_2N)_2$/TMHA-Tf_2N and 0.5 mol dm^{-3} $Mg(Tf_2N)_2$/PP13-Tf_2N (molar ratio 1 : 7) by mixing under an inert atmosphere in a glove box, and then we mixed these IL solutions with diglyme (1 : 4 by volume or 1 : 56 by mole) in the glove box to make 0.1 mol dm^{-3} Mg^{2+}-containing IL/G2 solutions.

Conductivity and viscosity measurements.— The water content of each solution was about 200 – 400 ppm, determined by Karl Fischer titration. Conductivity measurements were performed at 25°C using Radiometer Analytical CDM230. Kinematic viscosity measurements were conducted using SEKONIC VM-10A and VM-1 G calibrated using a standard solution (NIPPON GREASE Co., Ltd.). The densities of 0.5 mol dm^{-3} Mg^{2+}-containing ILs were calculated to be 1.41 g cm^{-3} for TMHA-Tf_2N and 1.46 g cm^{-3} for PP13-Tf_2N using the measured value of weight and volume, while those of G2-mixed solutions were assumed to be 1.03–1.04 g cm^{-3} for 0.1 mol dm^{-3} $Mg(Tf_2N)$ in IL/G2 and 1.01 g cm^{-3} for 0.125 mol dm^{-3} $Mg(Tf_2N)$ in G2 using the reported density of pure G2 (0.937 g cm^{-3}).

Electrochemical measurements and characterization of deposits.— Within an hour after bath preparation, electrochemical measurements were conducted in the glove box with a potentiostat/galvanostat (BAS, ALS ELECTROCHEMICAL ANALYZER 660C) at 30°C. Cyclic voltammetry (CV) was performed without stirring in an electrode cell
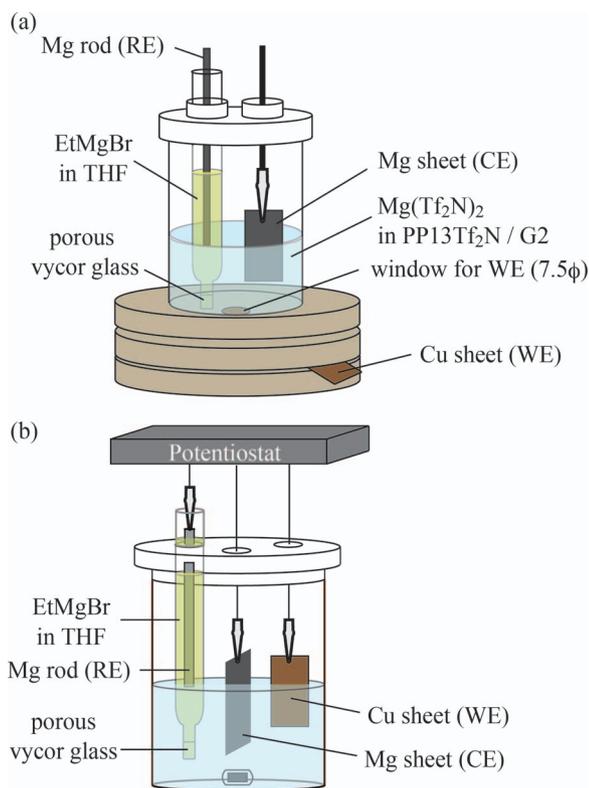
Figure 1. Schematic illustration of the cell configuration for (a) cyclic voltammetry and (b) potentiostatic electrolysis.

of 20 cm^3 capacity where the planar dimension of WE was fixed to 7.5 mmφ (Fig. 1a, EC Frontier, VM-2A). Potentiostatic electrolysis was conducted using a glass cell of 15 cm^3 capacity (Fig. 1b). Cu sheet (Nilaco, 99.9% purity) and Mg sheet or rod (Nilaco, 99.9% purity) were used as the working electrode (WE) and counter electrode (CE), respectively. Because the potential of Mg was not stable in some Tf$_2$N-based ILs,[26] as reference electrodes (RE) we used a Mg rod immersed in ethylmagnesium bromide (EtMgBr) in THF (Kanto Chemical, 0.95 mol dm^{-3}), separated from the main electrolyte by porous vycor glass (see Fig. 1). For CV measurements Cu sheets were washed with acetone, while for potentiostatic electrolysis they were first washed with acetone and then with about 1 mol dm^{-3} nitric acid before use. Mg sheets were polished with emery paper (#800) before measurements. In the potentiostatic electrolysis, dihedral angle of WE and CE was about 90° with a stirring speed of 300 rpm (see Fig. 1b). In order to characterize the deposits, X-ray diffraction (XRD) and scanning electron microscope (SEM) measurements were performed using RIGAKU RINT2200 and KEYENCE VE-7800, respectively.

Results and Discussion

Bath properties.— Table I shows the conductivities and kinematic viscosities of pure TMHA-Tf$_2$N and Mg(Tf$_2$N)$_2$ solutions in TMHA-Tf$_2$N and/or G2. The kinematic viscosity of 0.5 mol dm^{-3} Mg(Tf$_2$N)$_2$

Table I. Molar ratio, molar concentrations (*C*), conductivities (σ) and kinematic viscosities (η) of TMHA-Tf$_2$N and Mg(Tf$_2$N)$_2$-containing TMHA-Tf$_2$N and/or G2 solutions measured at 25°C.
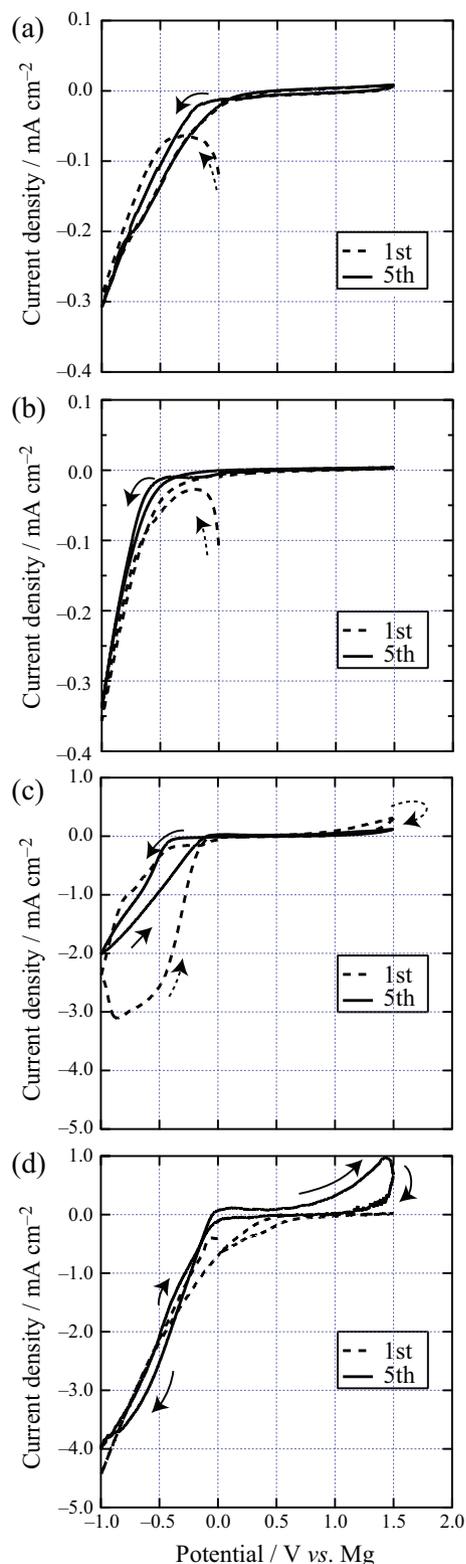
Molar ratio of Mg(Tf$_2$N)$_2$:TMHA-Tf$_2$N:G2	*C* (mol dm^{-3})	σ (mS cm^{-1})	η (mm^2 s^{-1})
0 : 1 : 0	-	4.9	1.31×10^2
1 : 7 : 0	0.5	0.35	6.35×10^2
1 : 7 : 56	0.1	2.5	2.19
1 : 0 : 56	0.125	0.50	1.31

Table II. Molar ratio, molar concentrations (*C*), conductivities (σ) and kinematic viscosities (η) of PP13-Tf$_2$N and Mg(Tf$_2$N)$_2$-containing PP13-Tf$_2$N and/or G2 solutions measured at 25°C.

Molar ratio of Mg(Tf$_2$N)$_2$:PP13-Tf$_2$N:G2	*C* (mol dm^{-3})	σ (mS cm^{-1})	η (mm^2 s^{-1})
0 : 1 : 0	-	5.6	1.16×10^2
1 : 7 : 0	0.5	0.35	4.02×10^2
1 : 7 : 56	0.1	2.6	2.23
1 : 0 : 56	0.125	0.50	1.31

in TMHA-Tf$_2$N (6.35×10^2 mm^2 s^{-1}) became about five times higher than pure TMHA-Tf$_2$N (1.31×10^2 mm^2 s^{-1}). By mixing with G2, the kinematic viscosity decreased by two orders of magnitude (2.19 mm^2 s^{-1}), which is comparable with that of the Mg^{2+}-G2 solution (1.31 mm^2 s^{-1}). The conductivity of the TMHA-Tf$_2$N-G2 solutions improved by an order of magnitude (2.5 mS cm^{-1}) compared to the other Mg(Tf$_2$N)$_2$ solutions and was only about half value for pure TMHA-Tf$_2$N (4.9 mS cm^{-1}). Such dilution effect by adding G2 was also seen in the case of PP13-Tf$_2$N (see Table II). The kinematic viscosity of 0.5 mol dm^{-3} Mg(Tf$_2$N)$_2$ in PP13-Tf$_2$N (4.02×10^2 mm^2 s^{-1}) was about four times higher than pure PP13-Tf$_2$N (1.16×10^2 mm^2 s^{-1}). By mixing with G2, the kinematic viscosity decreased by two orders of magnitude (2.23 mm^2 s^{-1}) from the case of 0.5 mol dm^{-3} Mg(Tf$_2$N)$_2$ in PP13-Tf$_2$N (4.02×10^2 mm^2 s^{-1}) and the conductivity improved by an order of magnitude (2.6 mS cm^{-1}) compared to the IL solution (0.35 mS cm^{-1}) or the G2 solution (0.50 mS cm^{-1}). As a result, the IL-G2 mixture gave better results than the other Mg^{2+}-containing solutions.

Cyclic voltammetry.— Figure 2 shows the CVs measured in several electrolytes. As shown in Fig. 2a, 2b, before adding G2, the CVs show reduction currents of about –0.3 mA cm^{-2} at –1.0 V vs. Mg and only a little oxidation currents. In contrast, mixing Mg-containing ILs with G2 caused a drastic increase in the current density (by an order of magnitude) and sizable decrease in the overpotentials (see Fig. 2c, 2d). These results can be mainly attributed to the following two reasons. The first is a dilution effect, where the mobility of Mg^{2+} cations becomes much larger when glymes are added, as proposed in the case of Li$^+$.[27] The second is the possible change in coordination geometry, where Mg^{2+} cations are coordinated by G2 molecules instead of Tf$_2$N$^-$ anions. It has been reported that some strong Lewis acids such as Li$^+$ and Zn^{2+} are coordinated by Tf$_2$N$^-$ anions in the ILs, and exist in the form of monovalent [Li(Tf$_2$N)$_2$]$^-$ and [Zn(Tf$_2$N)$_3$]$^-$ anions.[28–30] Because the ionic radius of Mg^{2+} (89 pm) is similar to that of Li$^+$ (92 pm), it would exist in the form of [Mg(Tf$_2$N)$_3$]$^-$ in the IL solutions without glymes, while in the presence of glymes they would solvate and form Mg^{2+}-G2 complex cations (e.g. [Mg(G2)$_n$]$^{2+}$) like Li$^+$-glyme complexes.[31–33] If Mg^{2+}-glyme complex cations were formed, they may more easily access the cathode surface compared to [Mg(Tf$_2$N)$_3$]$^-$ because of the electrostatic attractions with cathode. Another possibility is that the complex of Mg^{2+} and Tf$_2$N$^-$ can hardly desolvate because of electrostatic attraction, while glymes with neutral charge may more easily desolvate from Mg^{2+}, even though it should be thermodynamically disadvantageous compared to Tf$_2$N complex. Although we obtained large reduction currents in the cases of both TMHA-Tf$_2$N/G2 and PP13-Tf$_2$N/G2 (see Fig. 2c, 2d), their oxidation currents were relatively small, suggesting that dissolution of Mg was prohibited possibly because Tf$_2$N$^-$ anions developed passivation films on the deposited Mg, as previously indicated in some organic and Tf$_2$N-type IL solutions of Mg(Tf$_2$N)$_2$.[34–37] Nonetheless, among these Mg^{2+}-containing baths, PP13-Tf$_2$N/G2 showed the largest reduction and oxidation currents and did not decay up to the 5th cycles (see Fig. 2d). Figure 3 shows the electrochemical window for PP13-Tf$_2$N/G2 without Mg(Tf$_2$N)$_2$ using Cu as WE, Mg in Grignard as RE, and glassy carbon as CE. The Mg^{2+}-free electrolyte undergoes reduction at ca. –0.7 V and oxidation

Figure 3. CV (from 0 V to –1.5 V to +3 V to 0 V; 20 mV s^{-1}) showing the electrochemical window for Mg^{2+}-free PP13-Tf$_2$N/G2, where Cu was used as WE, Mg in THF solution of EtMgBr was used as RE, and glassy carbon was used as CE.

sition of Mg metal from the PP13-Tf$_2$N/G2 mixture that showed the largest current density and the smallest overpotential of Mg electrodeposition.

Potentiostatic electrodeposition.— Figure 4a shows the *I-t* curve for the cathodic deposition at –1.0 V in the PP13-Tf$_2$N/G2 mixture. The cathodic current density at the beginning was as high as about 7.5 mA cm^{-2} and became higher with time, reaching the order of 10 mA cm^{-2} after 30 min. This implies that the effective surface area for deposition became larger and larger with time. Shown in Fig. 4b is a photograph of the Cu WE and Mg CE after electrolysis at –1.0 V; the WE Cu sheet is coated by silver-colored material with a metallic
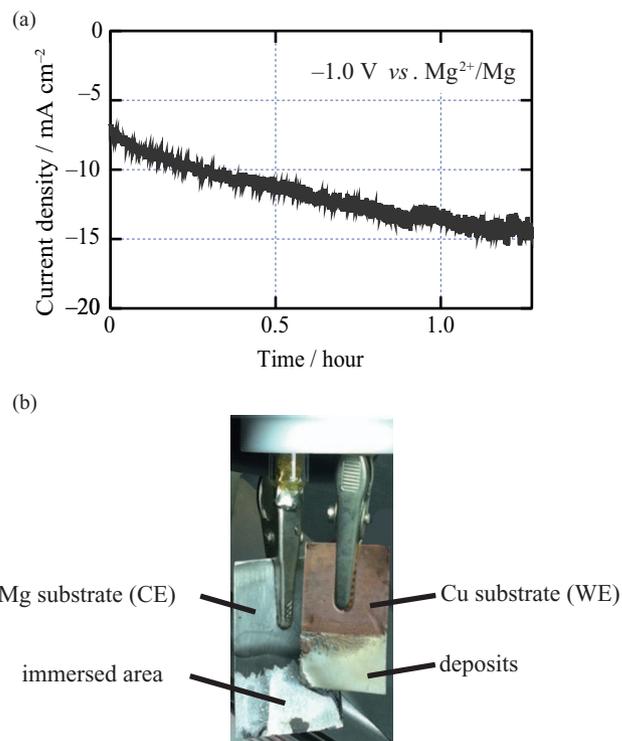
Figure 4. (a) *I-t* curves obtained at –1.0 V vs. Mg^{2+}/Mg with a stirring speed of 300 rpm at 30°C in the PP13-Tf$_2$N/G2 mixture (1 : 4 by volume) where 0.1 mol dm^{-3} Mg(Tf$_2$N)$_2$ dissolved, and (b) photograph of WE and CE after electrodeposition.

Figure 2. Cyclic voltammograms measured for 0.5 mol dm^{-3} Mg(Tf$_2$N)$_2$ in (a) TMHA-Tf$_2$N, (b) PP13-Tf$_2$N, and 0.1 mol dm^{-3} Mg(Tf$_2$N)$_2$ in (c) TMHA-Tf$_2$N/G2 and (d) PP13-Tf$_2$N/G2. Sweep rate: 20 mV s^{-1}.

i.e. bath decomposition and anodic dissolution of Cu WE at ca. +2.4 V, respectively. These results strongly indicate that the observed reduction and oxidation current in Fig. 2d strongly indicate deposition and dissolution of Mg metal. Therefore we attempted electrodepo-
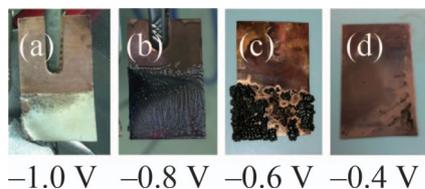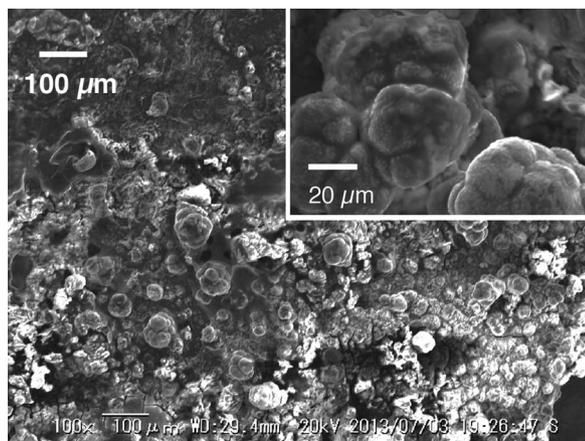
Figure 5. Photographs of WE after electrodeposition at (a) −1.0 V, (b) −0.8 V, (c) −0.6 V, and (d) −0.4 V vs. Mg.

Figure 7. XRD profile of the Cu sheet after electrodeposition at −1.0 V vs. Mg^{2+}/Mg in 0.1 mol dm^{-3} PP13-Tf$_2$N/G2 (upper panel) and calculated intensity ratio of Mg (JCPDS 00-004-0770) (lower panel).

luster and the immersed area of the CE Mg sheet became brighter than before, strongly indicating success in electrodeposition of Mg at the WE and anodic dissolution of Mg at the CE. The coulombic efficiency for deposition at −1.0 V was calculated to be about 100% from the mass change when we used a polished Mg sheet as WE. In general, at higher potentials or lower cathodic currents, more flat deposition can be obtained. However, as shown in Figure 5, potentiostatic electrolysis at higher than −1.0 V, i.e. −0.8 V, −0.6 V, and −0.4 V did not result in flat deposition. The observed nonuniform deposition suggests that nucleation of Mg on Cu is much more difficult at the lower potentials, while the deposition at −1.0 V enabled non-localized Mg nucleation on Cu substrate. As a result, relatively flat electrodeposition of Mg at a high growth rate was achieved.

Characterization of deposits.— Figure 6 shows SEM images of the Mg deposits; they are round in shape, different from a typical dendritic morphology, similar to those obtained from Grignard electrolytes.[38] Shown in Fig. 7 is the XRD pattern of WE after electrodeposition, which confirms that the deposits consisted of elemental Mg without any Mg-Cu alloy formation or sizable impurities; notably, however, the intensity ratio of the 002 peak was much weaker than the standard one. Matsui discussed the orientation of Mg deposits obtained in Grignard solutions, where ⟨100⟩ orientation was observed at a high deposition rate of 2 mA cm^{-2}, probably due to the different crystal growth rate in the hexagonal structure.[38] Because the deposition current in the glyme-IL solution was as high as about 10 mA cm^{-2}, our result is consistent with Ref. 38.

Possibility for battery application.— Here we remark whether the PP13-Tf$_2$N-G2 mixture could be used for Mg ion secondary batteries. Fig. 2d strongly suggests the formation of passivation film on Mg negative electrode, which is not suitable for battery application. However, with the scan rate of 20 mV s^{-1}, the anodic current is appreciable even at around 0 V, indicating that the formation of passivation film is time dependent. Therefore, one can say that as long as the charging/discharging rate is fast enough, this IL-containing
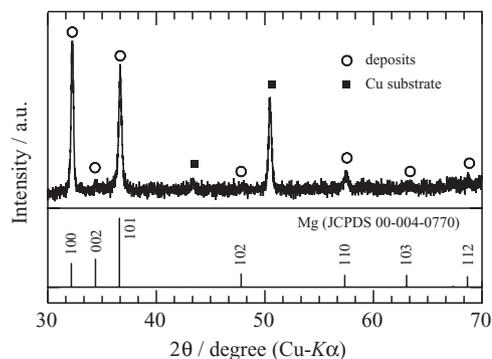
diglyme solution can possibly be used for battery application. Moreover, in charging process, the electrolyte is advantageous in that one can perform fast and flat deposition of Mg negative electrode at room temperature.

Conclusions

In this work, we demonstrated electrodeposition of Mg metal from Mg(Tf$_2$N)$_2$ in an IL-glyme mixture at room temperature. We revealed that addition of an IL to glyme considerably increased the conductivity, and is very effective for increasing the reduction current. It is likely suggested that glymes coordinate with Mg^{2+} cations instead of Tf$_2$N anions in the glyme-IL mixture and reduce the interfacial resistance. The safety of the plating bath has improved compared to Grignard reagents reported previously. In addition, the rapid and flat electrodeposition of Mg metal at room temperature is meaningful. Although the anodic current was relatively small, the amide-type-IL/glyme electrolytes potentially open a new option for Mg-ion secondary battery electrolytes. Further studies on the redox behavior of metallic Mg using other combinations of IL/glyme solutions that contain less glyme are under way.

References

1. P. Jolibois, *Compt. Rend.*, **155**, 353 (1912).
2. N. W. Kondyrew, *Chem. Ber.*, **58**, 459 (1925).
3. N. W. Kondyrew and D. P. Manojew, *Chem. Ber.*, **58**, 464 (1925).
4. L. W. Gaddum and H. E. French, *J. Am. Chem. Soc.*, **49**, 1295 (1927).
5. D. M. Overcash and F. C. Mathers, *Trans. Electrochem. Soc.*, **64**, 305 (1933).
6. J. H. Conner, W. E. G. Reid, and B. Wood, *J. Electrochem. Soc.*, **104**, 38 (1957).
7. C. Liebenow, *J. Appl. Electrochem.*, **27**, 221 (1997).
8. C. Liebenow, Z. Yang, and P. Lobitz, *Electrochem. Commun.*, **2**, 641 (2000).
9. D. Aurbach, A. Schechter, M. Moshkovich, and Y. Cohen, *J. Electrochem. Soc.*, **148**, A1004 (2001).
10. D. Aurbach, R. Turgeman, O. Chusid, and Y. Gofer, *Electrochem. Commun.*, **3**, 252 (2001).
11. Y. Viestfrid, M. D. Levi, Y. Gofer, and D. Aurbach, *J. Electroanal. Chem.*, **576**, 183 (2005).
12. Y. Gofer, O. Chusid, H. Gizbar, Y. Viestfrid, and H. E. Gottlieb, *Electrochem. Solid-State Lett.*, **9**, A257 (2006).
13. O. Mizrahi, N. Amir, E. Pollak, O. Chusid, V. Marks, H. Gottlieb, L. Larush, E. Zinigrad, and D. Aurbach, *J. Electrochem. Soc.*, **155**, A103 (2008).
14. N. Amir, Y. Vestfrid, O. Chusid, Y. Gofer, and D. Aurbach, *J. Power Sources*, **174**, 1234 (2007).
15. D. Aurbach, H. Gizbar, A. Schechter, O. Chusid, H. E. Gottlieb, Y. Gofer, and I. Goldberg, *J. Electrochem. Soc.*, **149**, A115 (2002).

Figure 6. SEM images of Mg deposits obtained at −1.0 V vs. Mg^{2+}/Mg from the PP13-Tf$_2$N/G2 mixture bath.

16. H. S. Kim, T. S. Arthur, G. D. Allred, J. Zajicek, J. G. Newman, A. E. Rodnyansky, A. G. Oliver, W. C. Boggess, and J. Muldoon, *Nat. Commun.*, **2**, (2011).
17. N. Yoshimoto, M. Matsumoto, M. Egashira, and M. Morita, *J. Power Sources*, **195**, 2096 (2010).
18. G. T. Cheek, W. E. O'Grady, S. Z El Abedin, E. M. Moustafa, and F. Endres, *J. Electrochem. Soc.*, **155**, D91 (2008).
19. M. Shiraga, F. Sagane, K. Miyazaki, T. Fukutsuka, T. Abe, K. Nishio, and Y. Uchimoto, Abstract 52, *The Electrochemical Society Meeting Abstracts*, Vol. 2010-02, Honolulu, USA, Oct 11, 2010.
20. R. Yasui, K. Asaka, K. Miyazaki, T. Fukutsuka, T. Abe, K. Nishio, and Y. Uchimoto, *Abstracts of the Electrochemical Society of Japan*, **80**, 238 (2013).
21. Y. NuLi, J. Yang, and R. Wu, *Electrochem. Commn.*, **7**, 1105 (2005).
22. Y. NuLi, J. Yang, J. Wang, J. Xu, and P. Wang, *Electrohem. Solid-State Lett.*, **8**, C166 (2005).
23. Y. NuLi, J. Yang, and P. Wang, *Appl. Surf. Sci.*, **252**, 8086 (2006).
24. Z. Feng, Y. NuLi, J. Wang, and J. Yang, *J. Electrochem. Soc.*, **153**, C689 (2006).
25. O. Shimamura, N. Yoshimoto, M. Matsumoto, M. Egashira, and M. Morita, *J. Power Sources*, **196**, 1586 (2011).
26. K. Murase, I. Sasaki, A. Kitada, T. Ichii, Y. Uchimoto, and H. Sugimura, *J. Electrochem. Soc.*, **160**(10), D453 (2011).
27. Y.-L. Zhu, Y. Kozuma, Y. Katayama, and T. Miura, *Elechtrochim. Acta*, **54**, 7502 (2009).
28. J.-C. Lassègues, J. Grondin, and D. Talaga, *Phys. Chem. Chem. Phys.*, **8**, 5629 (2006).
29. Y. Umebayashi, T. Mitsugi, S. Fukuda, T. Fujimori, K. Fujii, R. Kanzaki, M. Takeuchi, and S. Ishiguro, *J. Phys. Chem. B*, **111**, 13028 (2007).
30. K. Fujii, T. Nonaka, Y. Akimoto, Y. Umebayashi, and S. Ishiguro, *Anal. Sci.*, **24**, 1377 (2008).
31. T. Tamura, K. Yoshida, T. Hachida, M Tsuchiya, M. Nakamura, Y. Kazue, N. Tachikawa, K. Dokko, and M. Watanabe, *Chem. Lett.*, **39**, 753 (2010).
32. T. Tamura, T. Hachida, K. Yoshida, N. Tachikawa, K. Dokko, and M. Watanabe, *J. Power Sources*, **195**, 6095 (2010).
33. Y. Katayama, S. Miyashita, and T. Miura, *J. Power Sources*, **195**, 6162 (2010).
34. D. Aurbach, I. Weissman, Y. Gofer, and E. Levi, *Chem. Rec.*, **3**, 61 (2003).
35. M. Forsyth, P. C. Howlett, S. K. Tan, D. R. MacFarlane, and N. Birbilis, *Electrochem. Solid-State Lett.*, **9**, B52 (2006).
36. N. Birbilis, P. C. Howlett, D. R. MacFarlane, and M. Forsyth, *Surf. Coat. Technol.*, **201**, 4496 (2007).
37. M. Forsyth, W. C. Neil, P. C. Howlett, D. R. MacFarlane, B. R. W. Hinton, N. Rocher, T. F. Kemp, and M. E. Smith, *ACS Appl. Mater. Interfaces*, **1**, 1045 (2009).
38. M. Matsui, *J. Power Sources*, **196**, 7048 (2011).